

NRL Report 7991

An Analysis of the Breakup of Satellite 1974-103A (Cosmos 699)

WILLIAM B. HEARD

*Systems Research Branch
Space Systems Division*

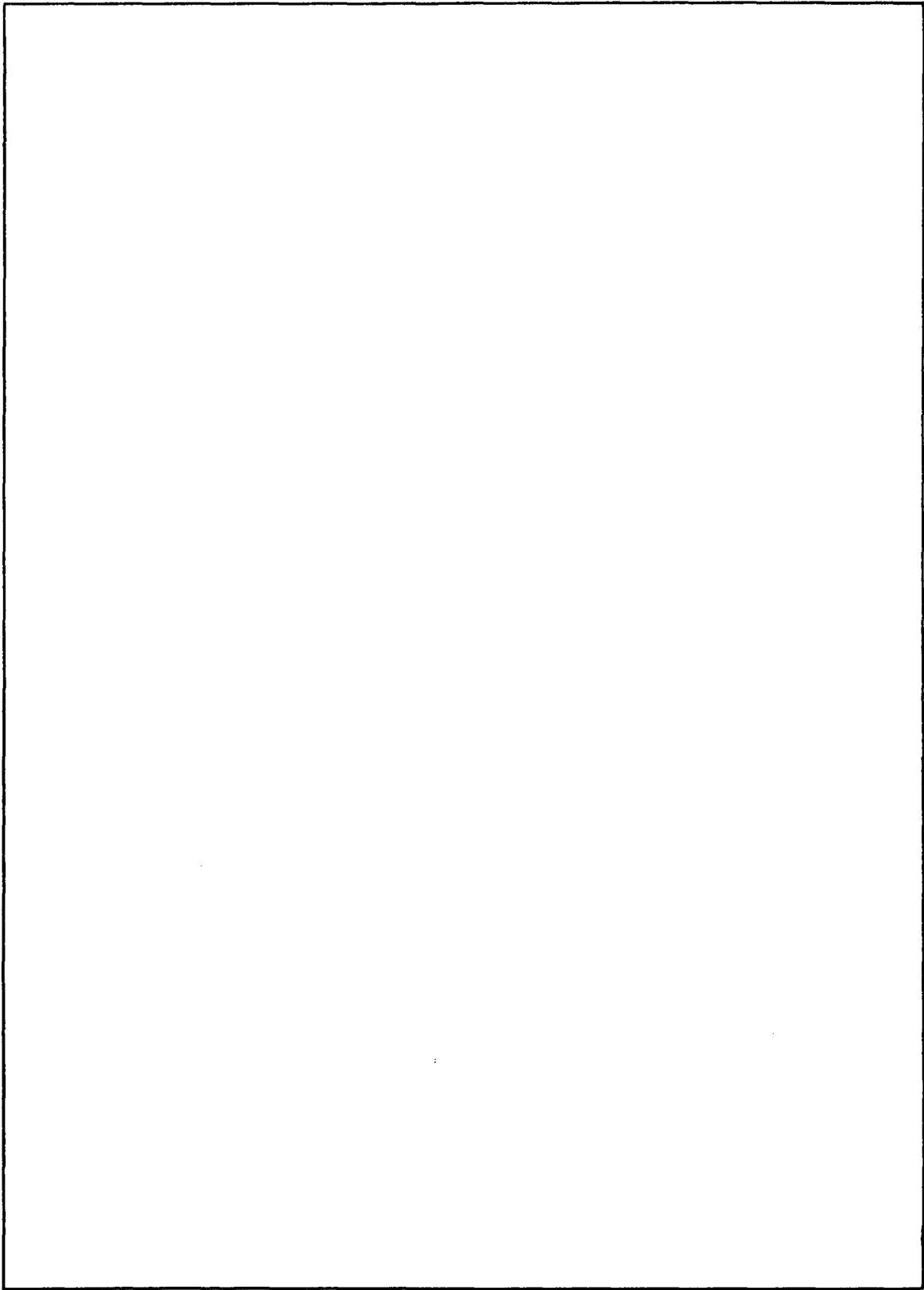
April 23, 1976



NAVAL RESEARCH LABORATORY
Washington, D.C.

Approved for public release; distribution unlimited.

REPORT DOCUMENTATION PAGE		READ INSTRUCTIONS BEFORE COMPLETING FORM
1. REPORT NUMBER NRL Report 7991	2. GOVT ACCESSION NO.	3. RECIPIENT'S CATALOG NUMBER
4. TITLE (and Subtitle) AN ANALYSIS OF THE BREAKUP OF SATELLITE 1974-103A (COSMOS 699)	5. TYPE OF REPORT & PERIOD COVERED Interim report on a continuing NRL Problem	
	6. PERFORMING ORG. REPORT NUMBER	
7. AUTHOR(s) William B. Heard	8. CONTRACT OR GRANT NUMBER(s)	
9. PERFORMING ORGANIZATION NAME AND ADDRESS Naval Research Laboratory Washington, D. C. 20375	10. PROGRAM ELEMENT, PROJECT, TASK AREA & WORK UNIT NUMBERS NRL Problem 301-10 Project RR003-02-41-6152	
11. CONTROLLING OFFICE NAME AND ADDRESS Office of Naval Research Arlington, Va. 22217	12. REPORT DATE April 23, 1976	
	13. NUMBER OF PAGES 20	
14. MONITORING AGENCY NAME & ADDRESS (if different from Controlling Office)	15. SECURITY CLASS. (of this report) Unclassified	
	15a. DECLASSIFICATION/DOWNGRADING SCHEDULE	
16. DISTRIBUTION STATEMENT (of this Report) Approved for public release, distribution unlimited		
17. DISTRIBUTION STATEMENT (of the abstract entered in Block 20, if different from Report)		
18. SUPPLEMENTARY NOTES		
19. KEY WORDS (Continue on reverse side if necessary and identify by block number) Satellite breakup Artificial earth satellites Cosmos 699 Liouville theorem Space surveillance		
20. ABSTRACT (Continue on reverse side if necessary and identify by block number) The theory of satellite breakup based on statistical mechanics is extended in the area of the inverse problem and is applied to the 17 April 1975 breakup of Cosmos 699. The breakup is shown to be highly nonisotropic. In addition to the main event, there is evidence for smaller breakups separated from it by intervals of -2, +1, and +3 revolutions.		



CONTENTS

INTRODUCTION	1
THE OBSERVATIONAL DATA	1
THEORETICAL DEVELOPMENT	7
ANALYSIS OF FIRST MOMENTS	10
ANALYSIS OF SECOND MOMENTS	12
CONCLUSIONS	13
ACKNOWLEDGMENTS	15
REFERENCES	17

AN ANALYSIS OF THE BREAKUP OF SATELLITE 1974-103A (COSMOS 699)

INTRODUCTION

On 17 April 1975 the Department of Defense Space Surveillance System (NAVSPASUR, operated by the Navy, and SPADATS, operated by the Air Force) observed that satellite 1974-103A (Cosmos 699) had disintegrated into several fragments. According to the NASA Goddard Satellite Situation Report, SPADATS identified 50 objects associated with this breakup. Orbits for 38 fragments were determined by NAVSPASUR in the course of their analysis of the event.

The breakup of Cosmos 699 occurred as the NRL Systems Research Branch of the Space Systems Division was investigating the dynamics of ensembles of particles such as would result from a satellite breakup. The investigation had shown that the application of statistical mechanics, as done in the continuum theory of stellar dynamics, was a particularly promising approach. The interest surrounding the Cosmos 699 breakup has made it a focal point for the testing of the newly developed statistical theory of satellite breakups.

This report describes an analysis of the Cosmos 699 breakup base on the application of statistical mechanics and using NAVSPASUR elements for observational data. A guiding principle of the analysis is to contrast at every opportunity results obtained from the individual elements and those obtained from the statistical structure of the cloud as a whole.

THE OBSERVATIONAL DATA

The analysis is based on orbital elements of individual fragments which were determined at NAVSPASUR Headquarters, Dahlgren, Virginia. Thirty-eight element sets were supplied. Of these, three were rejected because of anomalous mean motion rates, and two were rejected because the time of epoch was considered to be either too near or too far from time of break-up. Thus 33 element sets were retained for analysis. The elements are listed in Table 1. Element set 1 is for the original COSMOS 699 payload. This element set provides the reference or parent orbit for the analysis.

The NAVSPASUR differential corrections (DC's) which estimated the elements were based on direction-cosine measurements of the NAVSPASUR "fence." The average number of observations per DC was ten over a time span of 3 days. Roughly 2/3 of the observations were single-station direction-cosine measurements, and roughly 1/3 involved two or more stations, which permitted a determination of range by triangulation. The DC for each

Table 1 — Orbital Elements

No.	To (days)	Mean Anomaly (deg)	Mean Motion (rev/day)	Decay Coeff. (rad/herg ²)	Eccentric- ity	Argu- ment of Perigee (deg)	Longitude of Ascending Node (deg)	Inclin- ation (deg)
1	110.0	335.5510	15.4454	0.0051	0.00100	310.6776	56.3094	65.0404
2	110.0	359.0504	15.4351	0.0122	0.00048	279.2321	56.3158	65.0173
3	110.0	64.5858	15.3922	0.0155	0.00175	181.2430	56.3451	64.9356
4	110.0	335.3910	15.2546	0.0088	0.00782	166.9099	56.4975	64.9342
5	110.0	15.3752	15.3317	0.0030	0.00425	185.3580	56.3897	64.8417
6	110.0	264.2435	15.1835	0.0139	0.01078	184.6668	56.5601	64.9101
7	110.0	41.6927	15.3819	0.0183	0.00221	196.3839	56.3644	64.9645
8	110.0	57.0992	15.4052	0.0360	0.00131	197.9745	56.3354	64.9681
9	110.0	170.2737	15.4213	0.0057	0.00079	96.5992	56.2871	64.8971
10	110.0	182.5328	15.4322	0.0455	0.00047	92.5385	56.2991	64.9160
11	110.0	49.9472	15.4084	0.0104	0.00119	208.2318	56.3392	64.9862
12	110.0	55.4496	15.4031	0.1043	0.00155	196.1986	56.3412	64.9674
13	110.0	348.7623	15.4378	0.0122	0.00088	291.4285	56.3201	65.0201
14	110.0	98.6550	15.4135	0.0594	0.00097	161.9419	56.3186	64.9234
15	110.0	102.7159	15.3919	0.0923	0.00248	140.5360	56.3509	64.9434
16	110.0	42.9998	15.3886	0.0799	0.00195	198.3201	56.3573	64.9654
18	110.0	302.4745	15.1965	0.0226	0.01107	155.5604	56.4660	64.5325
19	110.0	71.0607	15.4077	0.0107	0.00102	186.5389	56.3369	64.9764
20	110.0	53.9622	15.4073	0.0402	0.00126	202.5364	56.3382	64.9787
21	110.0	30.7012	15.4212	0.0447	0.00097	236.1496	56.3247	64.9862
22	110.0	48.6885	15.3858	0.0256	0.00207	191.9969	56.3547	64.9530
23	110.0	224.7948	15.1155	0.0039	0.01379	172.9877	56.6363	64.8813
24	110.0	57.5153	15.3871	0.1657	0.00274	180.0411	56.3496	64.9064
25	111.0	16.1099	14.8794	0.0036	0.02512	159.4454	52.7553	64.6755
26	111.0	254.3241	15.4095	0.0584	0.00125	148.3192	52.0097	64.9407
27	111.0	203.8913	15.4003	0.0226	0.00132	191.0535	51.9310	64.8473
28	111.0	293.2920	15.4276	0.0312	0.00069	130.9905	51.9967	64.9656
29	112.0	345.7332	15.4077	0.0820	0.00120	197.0296	47.6891	64.9417
30	111.0	5.8121	15.2187	0.0107	0.00939	187.8631	52.2603	64.7772
31	112.0	109.9450	15.4336	0.0951	0.00069	110.0842	47.6631	64.9636
32	112.0	319.2130	15.4306	0.0267	0.00107	262.6812	47.6601	64.9739
33	110.0	152.3584	15.0732	0.4037	0.01797	203.9177	56.5967	64.4484
34	110.0	44.1956	15.4261	0.0244	0.00068	226.9592	56.3232	65.0006

element set used estimated the classical elements and the rate of change of mean motion which parameterizes the atmospheric drag perturbation. The rms value of the residuals for the DC's was typically 500 to 1000 meters.

For the present analysis the element sets were propagated by calculating two-body and secular perturbative effects. This introduces an inconsistency, because the complete Brouwer theory was used in the DC process at NAVSPASUR. However the differences (certainly less than 1 km) are insignificant for the purposes of this analysis.

The elements were found to fall into two classes. The first class consisted of 28 fragments which dispersed simultaneously from the parent body at 107^d.9083 (3.0°N, 82.9°W). The second class consisted of five fragments which apparently fragmented at different times. The second class will be discussed further in the concluding section.

The evolution of the positions of the fragments is shown in Figs. 1 through 8 during the first 1/2 revolution after breakup. The differences are resolved along the unit vectors

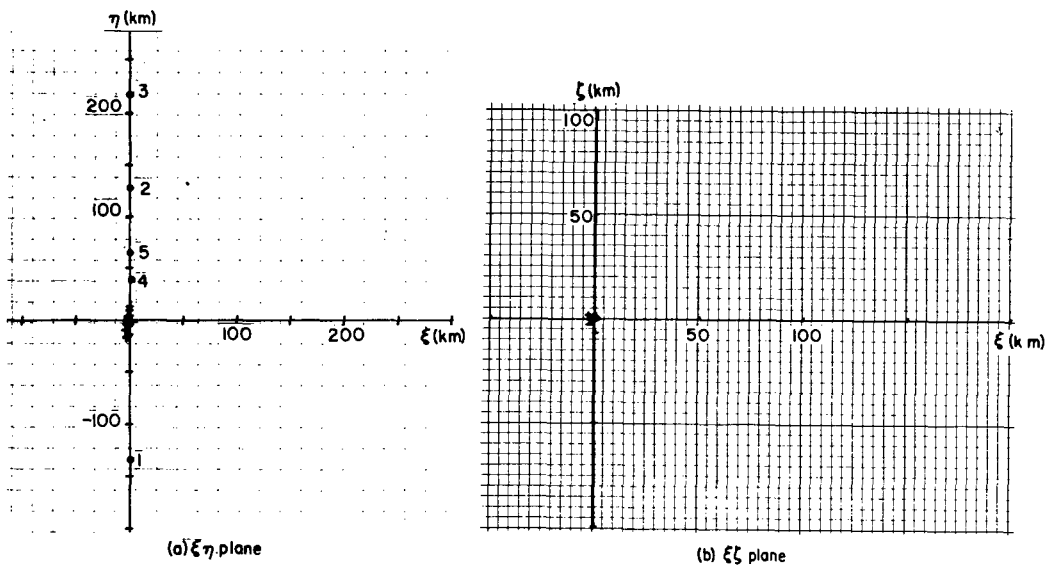


Fig. 1 — Position of fragments relative to the payload when $v - v_0 = 0.03$ radian (a) $\xi\eta$ plane (b) $\xi\zeta$ plane. Fragments 1 through 5 correspond to element sets 9, 29, 31, 32, and 33 respectively (Table 1).

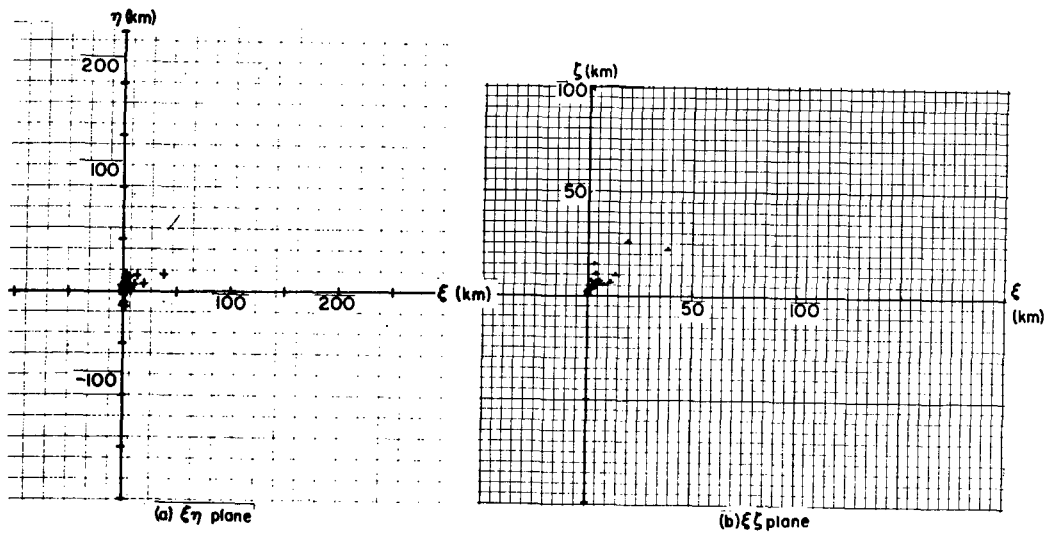


Fig. 2 — Position of fragments relative to the payload when $v - v_0 = 0.48$ radian (a) $\xi\eta$ plane (b) $\xi\zeta$ plane

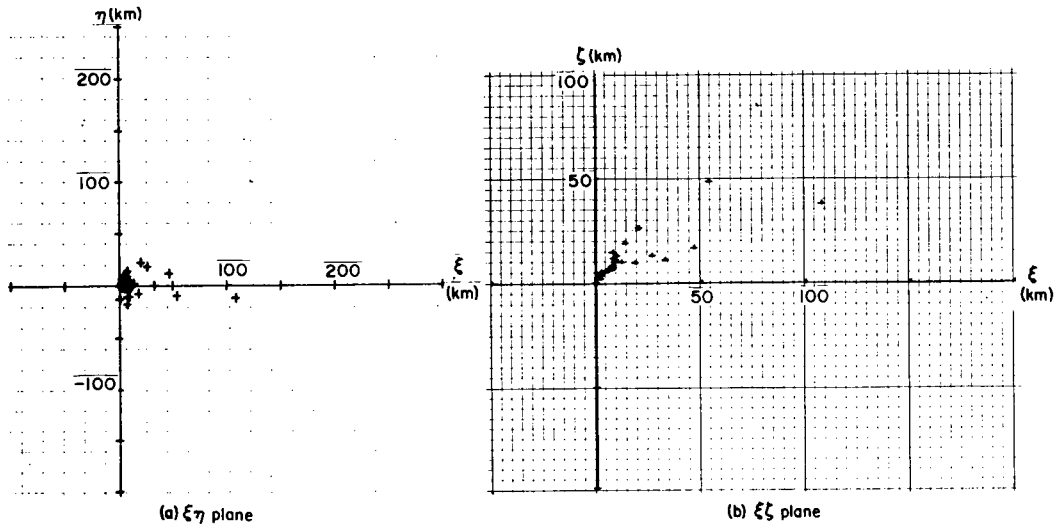


Fig. 3 — Position of fragments relative to the payload when $v - v_0 = 0.97$ radian
 (a) $\xi\eta$ plane (b) $\xi\zeta$ plane

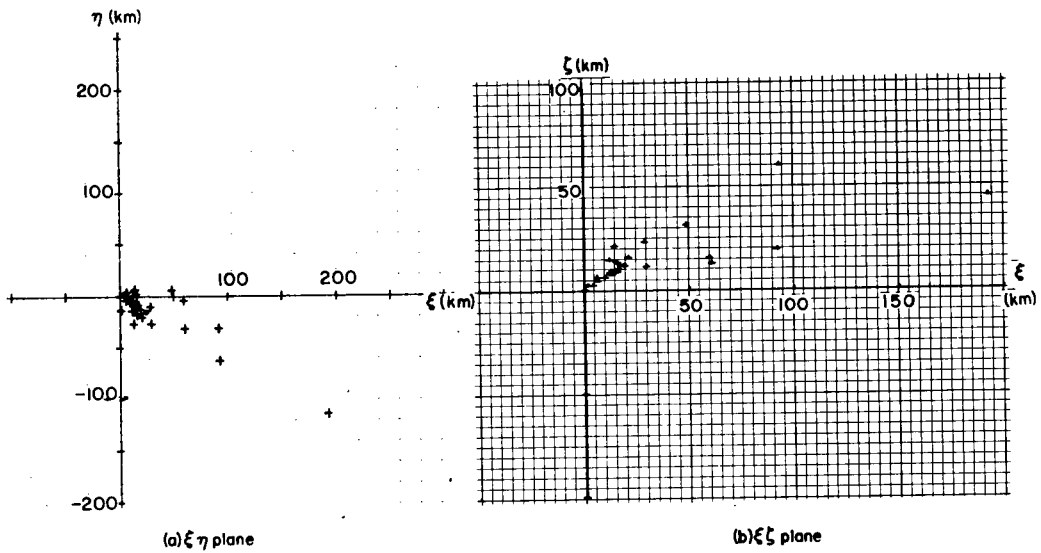


Fig. 4 — Position of fragments relative to the payload when $v - v_0 = 1.46$ radians
 (a) $\xi\eta$ plane (b) $\xi\zeta$ plane

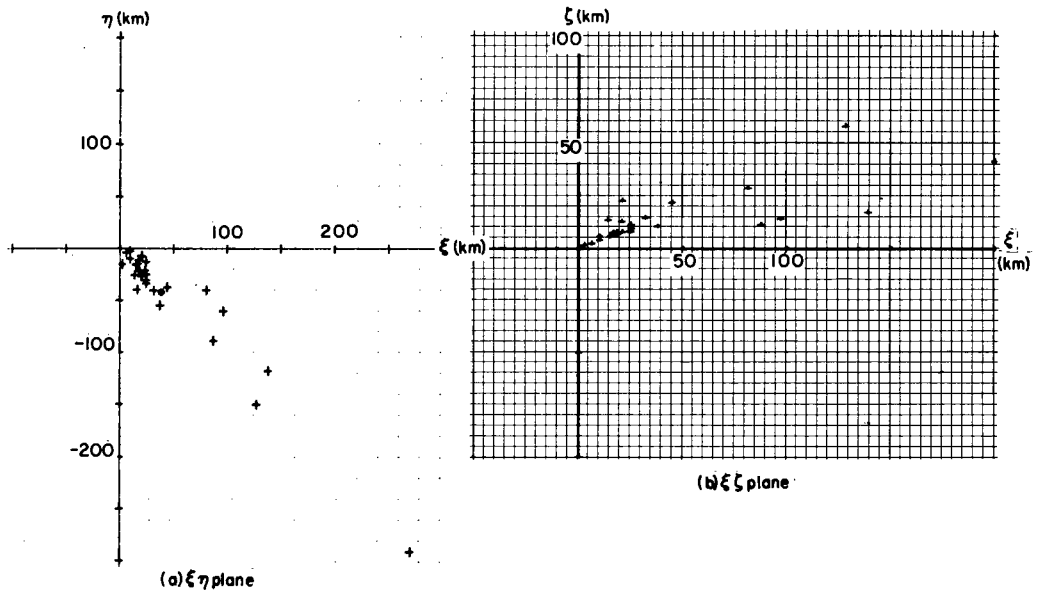


Fig. 5 — Position of fragments relative to the payload when $v - v_0 = 1.94$ radians
 (a) $\xi\eta$ plane (b) $\xi\zeta$ plane

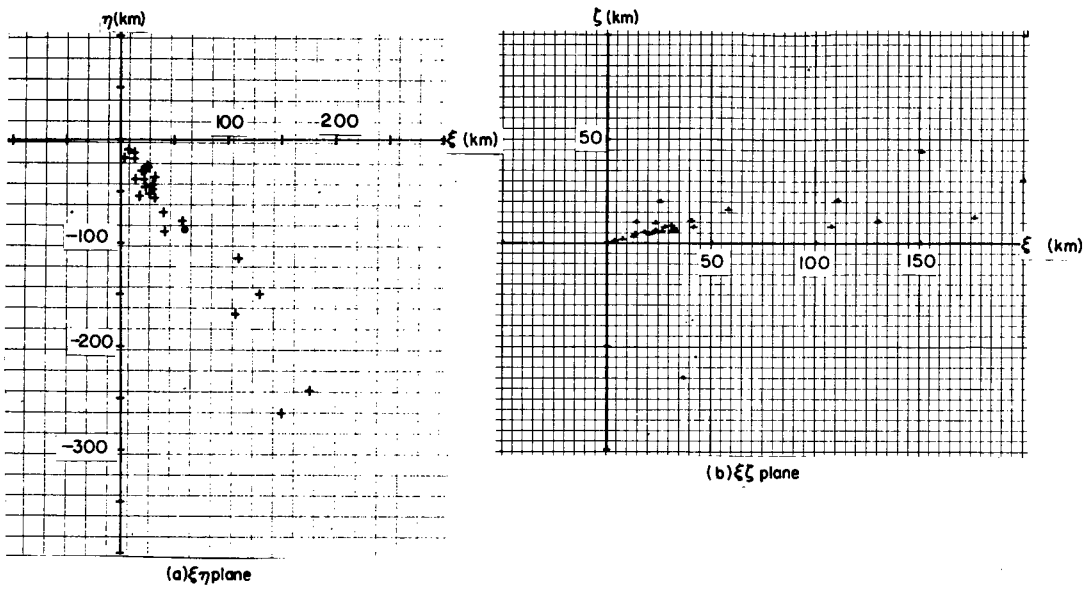


Fig. 6 — Position of fragments relative to the payload when $v - v_0 = 2.43$ radians
 (a) $\xi\eta$ plane (b) $\xi\zeta$ plane

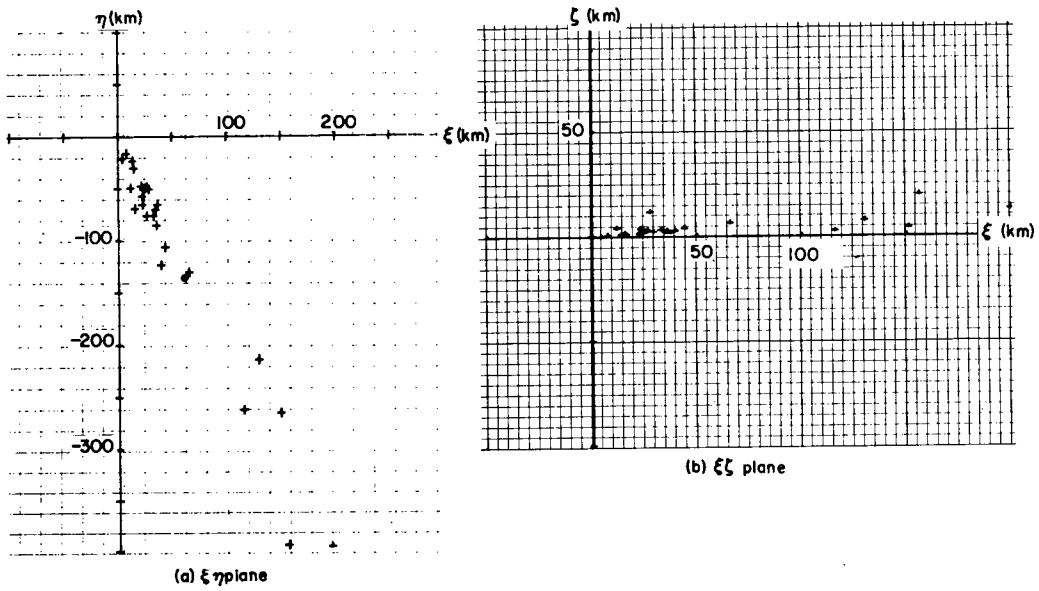


Fig. 7 — Position of fragments relative to the payload when $v - v_0 = 2.91$ radians
 (a) $\xi\eta$ plane (b) $\xi\zeta$ plane

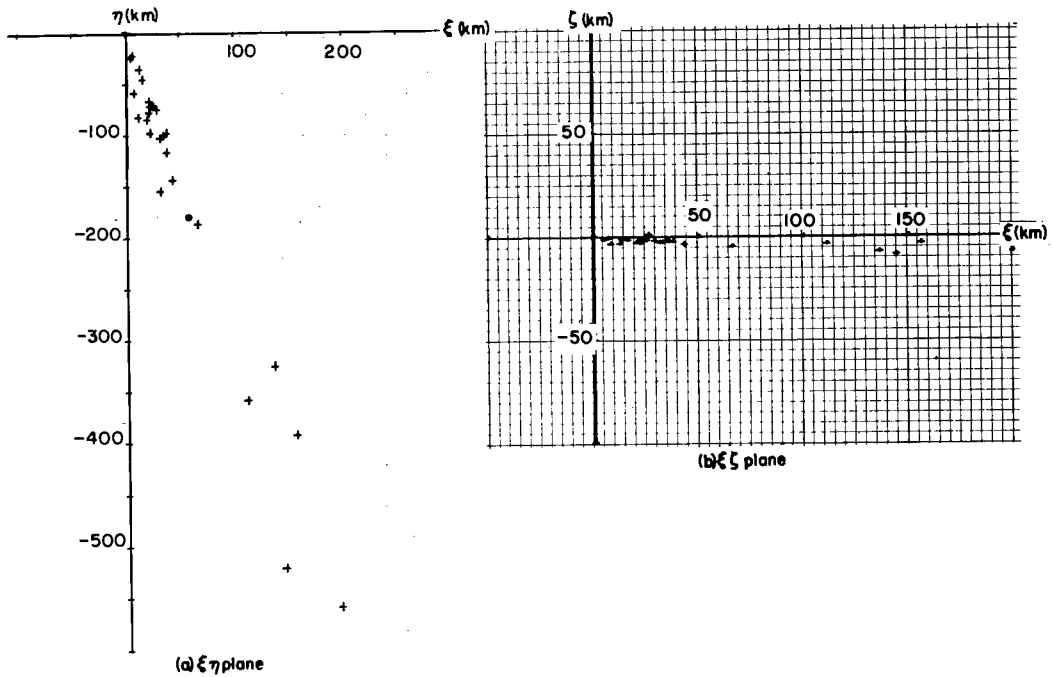


Fig. 8 — Position of fragments relative to the payload when $v - v_0 = 3.40$ radians
 (a) $\xi\eta$ plane (b) $\xi\zeta$ plane

$$\begin{aligned} \mathbf{e}_1 &= \mathbf{r} / |\mathbf{r}| && (\xi \text{ component}), \\ \mathbf{e}_3 &= \mathbf{r} \times \mathbf{v} / |\mathbf{r} \times \mathbf{v}| && (\zeta \text{ component}), \\ \mathbf{e}_2 &= \mathbf{e}_3 \times \mathbf{e}_1 && (\eta \text{ component}), \end{aligned}$$

where \mathbf{r} and \mathbf{v} are the position and velocity vectors of the parent. Figures 1a through 8a show the projection of the relative positions onto the $\xi \eta$ plane, and Figs. 1b through 8b show the projections onto the $\xi \zeta$ plane. The five fragments of the second class are indicated by the numbered filled circles in Fig. 1a.

THEORETICAL DEVELOPMENT

The theoretical basis for this analysis is the application of statistical mechanics to study ensembles of noninteracting particles [1]. There is however an area of the theory which must be expanded before we can proceed with the analysis. The inverse problem of determining the age and initial velocity distribution has been treated in detail only for a two-dimensional ellipsoidal breakup from a circular parent orbit. This must be extended to three dimensions in order to proceed. Thus this section is devoted to the inverse problem for a slowly dispersing three-dimensional ellipsoidal breakup. There is no reason for restriction to circular parent orbits in the theoretical development, but the eccentricity of Cosmos 699 was small enough that this simplification can be used in the application.

Statistical mechanics theory treats the ensemble of fragments as a continuum of particles described by a phase-space distribution function $f(\mathbf{q}, \mathbf{p}, t)$. If the equations of motion of the individual fragments are determined by the Hamiltonian $\mathcal{H}(\mathbf{q}, \mathbf{p}, t)$, then f satisfies Liouville's equation

$$\frac{\partial f}{\partial t} + (f, \mathcal{H}) = 0, \quad (1)$$

where (\cdot, \cdot) denotes the Poisson bracket. The initial condition satisfied for a body disintegrating at coordinate \mathbf{q}_* at $t = 0$ is

$$f(\mathbf{q}, \mathbf{p}, 0) = \delta(\mathbf{q} - \mathbf{q}_*) G(\mathbf{p}), \quad (2)$$

where $\delta(\cdot)$ is the Dirac delta function and $G(\mathbf{p})$ describes the initial distribution of momenta.

The equations of motion may be linearized about the reference trajectory if the particles disperse slowly or, equivalently, if the concern is with the initial phase of the breakup. Then the solution of the equations of motion becomes

$$\begin{pmatrix} \mathbf{q} \\ \mathbf{p} \end{pmatrix} = \begin{pmatrix} U & V \\ W & Y \end{pmatrix} \begin{pmatrix} \mathbf{q}_0 \\ \mathbf{p}_0 \end{pmatrix}. \quad (3)$$

As shown in Ref. 1 the solution for f becomes

$$f = \delta(U\mathbf{q} + V\mathbf{p} - \mathbf{q}_*) G(W\mathbf{q} + Y\mathbf{p}), \quad (4)$$

and the spatial density

$$\rho(\mathbf{q}, t) = \int f(\mathbf{q}, \mathbf{p}, t) d\mathbf{p} \quad (5)$$

becomes

$$\rho = \det(V_-^{-1}) G[(W_- - Y_- V_-^{-1} U_-) \mathbf{q} + Y_- V_-^{-1} \mathbf{q}_*], \quad (6)$$

where the notation $U(-t) = U_-(t)$, etc., is used. We may set $\mathbf{q}_* = 0$, because the breakup originates on the parent orbit.

The momentum distribution for an ellipsoidal breakup may be written

$$G(\mathbf{p}) = \text{const } e^{-(\mathbf{p} - \mathbf{p}_0) \cdot A(\mathbf{p} - \mathbf{p}_0)}. \quad (7)$$

The problem is to find the mean momentum \mathbf{p}_0 and the symmetric dispersion matrix A given the position of the fragments relative to the parent body as a function of time. To do this, the spatial density function is written as

$$\rho = K(t) e^{-F} \quad (8a)$$

with

$$K = (|\det V_-|)^{-1}, \quad (8b)$$

$$F = \mathbf{u} \cdot Q\mathbf{u}, \quad (8c)$$

$$\mathbf{u} = \mathbf{q} - M^{-1}\mathbf{p}_0, \quad (8d)$$

$$Q = M^T A M, \quad (8e)$$

and

$$M = W_- - Y_- V_-^{-1} U_-. \quad (8f)$$

The initial mean momentum is obtained immediately as

$$\mathbf{p}_0 = M\bar{\mathbf{q}},$$

where $\bar{\mathbf{q}}$ is the mean of the relative positions at time t . To obtain A , the matrix J is defined by

$$\text{ent}_{ij} J = \int \mathbf{u}_i \mathbf{u}_j \rho d\mathbf{u}. \quad (9)$$

This matrix is the point of contact with the observations and is obtained by calculating the second moments about the mean of the relative coordinates of the fragments. The theoretical value of the integral (9), assuming the ellipsoidal distribution (7), then relates A to the observables. If (8a) is substituted into (9), then [2] the result is

$$J = \frac{1}{2} \pi^{3/2} K (\det Q)^{-1/2} Q^{-1}. \quad (10)$$

The determinant of (10) yields the relation

$$(\det Q)^{-1/2} = \left(\frac{2}{\pi^{3/2} K} \right)^{3/5} (\det J)^{1/5}. \quad (11)$$

Therefore

$$Q = \left(\frac{\pi^{3/2} K}{2} \right)^{2/5} (\det J)^{1/5} J^{-1}. \quad (12)$$

Finally, from (8e),

$$A = (M^{-1})^T Q M^{-1}, \quad (13)$$

and this is the expression relating A to the observable J via equation (12).

The expressions (3) through (13) are valid for any linear dynamical system. The analysis here of Cosmos 699 however will be restricted to linearization about a circular Keplerian orbit. In this case explicit expressions for M^{-1} and K are

$$M^{-1} = \frac{1}{n} \begin{pmatrix} s & 2(1-c) & 0 \\ 2(c-1) & 4s-3nt & 0 \\ 0 & 0 & s \end{pmatrix}$$

and

$$K = \frac{n}{|s [-3nts + 8(1-c)]|},$$

where $s = \sin nt$, $c = \cos nt$, and n is the mean motion of the parent orbit. Equation (11) also provides an algorithm for estimating the age of the breakup. From equation (8e)

$$(\det Q)^{-1} \propto \det M^{-1}.$$

Therefore from equation (11)

$$(\det J)^{1/5} \propto \left(\frac{\pi^{3/2} K}{2} \right)^{3/5} (\det M^{-1}). \quad (16)$$

The left-hand side of (16) is obtained directly from the observations as a function of clock time. The right-hand side is a known function of time since breakup. The time of breakup is determined by translating the left-hand side in time to match the right-hand side. The translation determines time since breakup and therefore determines the breakup time itself. Since the reference orbit is known, knowledge of breakup time immediately provides the breakup position.

ANALYSIS OF FIRST MOMENTS

In this section, which begins the analysis of the Cosmos 699 data, the first moments, or means, of the relative positions of the fragments are analyzed. According to the theory in its linear approximation, the center of mass of the fragment ensemble will execute an epicycle in the reference plane. The out-of-plane motion is harmonic and is decoupled from the in-plane components. The observed epicyclic/harmonic motion will be used to determine both the mean of the initial velocity components and breakup age. The virtue of analyzing the fragment ensemble as a whole as opposed to straightforward statistics derived from the NAVSPASUR elements is that the former minimizes the effect of error that is inevitably present in the orbit-determination process. The velocity differences at breakup are comparable to the error expected in individual elements. However the extent of the ensemble cloud approximately 1/4 revolution after breakup far exceeds the error expected in the elements. Thus one can obtain reliable direct estimates of the structure of the fragment ensemble as opposed to unreliable direct estimates of the velocity differences at breakup time. The statistical theory enables one to translate the former into information about conditions at breakup time.

The mean of the ζ component versus time is shown in Fig. 9. The data fit the sine curve

$$\bar{\zeta} = 14.4 \sin(v - v_0 - 0.03).$$

The theoretical expression for this mean is

$$\bar{\zeta} = (\bar{\xi}_0/n) \sin[n(t - t_0)].$$

The clock times associated with the difference in true anomaly $v - v_0$ and the mean motion of the parent ($n = 0.001123$ rad/s) yields

$$\bar{\xi}_0 = 16.2 \text{ m/s}$$

and

$$t_0 = 107^d.9083.$$

The mean of ξ versus the mean of η is shown in Fig. 10. The theoretical expression for this curve is given parametrically by

$$\bar{\xi} = (\bar{\xi}_0/n) \sin[n(t - t_0)] + (2\bar{\eta}_0/n) \{1 - \cos[n(t - t_0)]\}$$

and

$$\bar{\eta} = (-2\bar{\xi}_0/n) \{1 - \cos[n(t - t_0)]\} + (\bar{\eta}_0/n) \{4 \sin[n(t - t_0)] - 3n(t - t_0)\}.$$

The data are well fit by the theoretical curve with

$$\bar{\xi}_0 = 4 \text{ m/s}$$

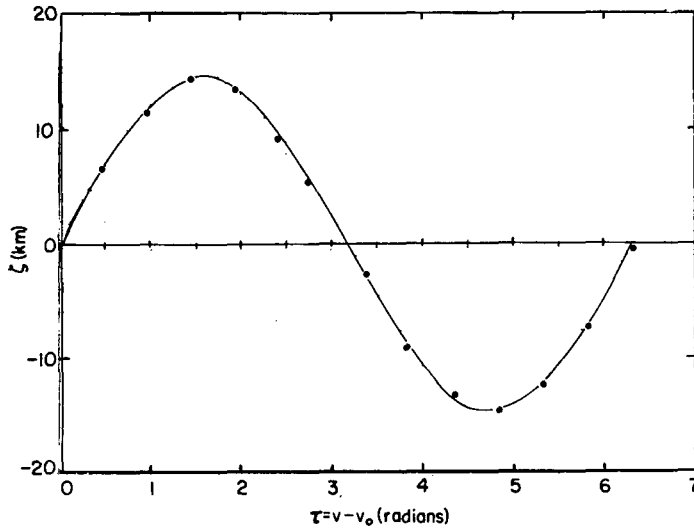


Fig. 9 — Average ζ coordinate versus true anomaly difference τ

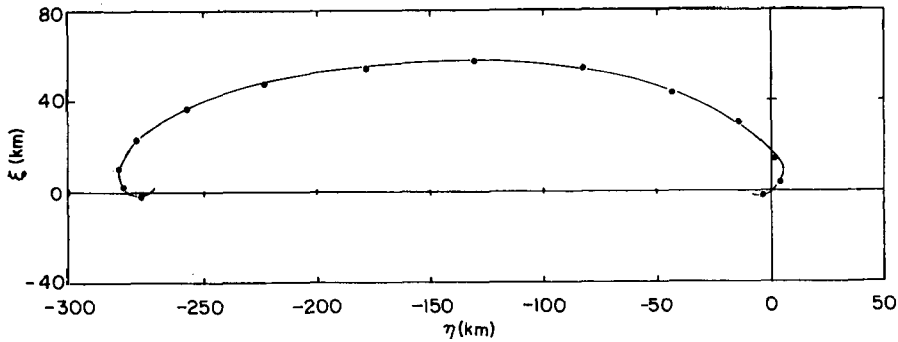


Fig. 10 — Average ξ coordinate versus the average η coordinate

and

$$\bar{\eta}_0 = 16.6 \text{ m/s.}$$

The amplitude of the sine curve and the epicycle are quite sensitive to $\bar{\xi}_0$ and $\bar{\eta}_0$ respectively. Consequently the uncertainties in these values are less than 0.2 m/s. The value of $\bar{\xi}_0$ is more difficult to estimate. The timing along the epicycle is the parameter most sensitive to $\bar{\xi}_0$. The value given is probably accurate to 1 m/s.

In Fig. 11 are shown the resolutions of the plane components of velocity residuals. Also shown are the estimated values of $\bar{\xi}_0$ and $\bar{\eta}_0$. They are seen to be consistent. However a straightforward calculation of $\bar{\xi}_0$ and $\bar{\eta}_0$ from these data produces an epicycle which fits the data poorly. Hence this is the first example of the advantage of the statistical theory with regard to observational error.

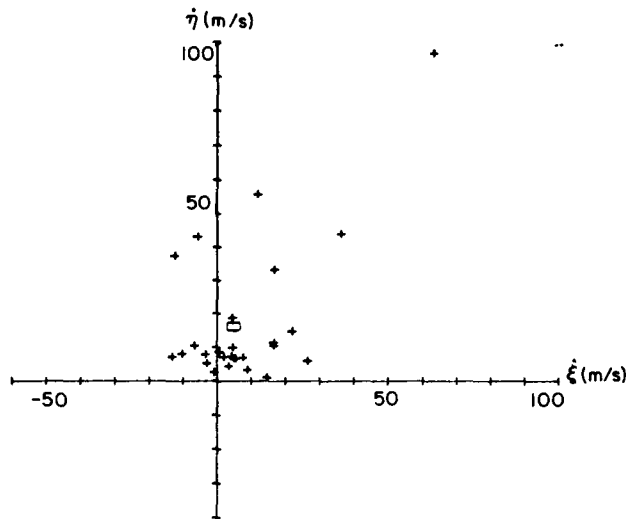


Fig. 11 — Projection of the velocity difference at breakup time onto the $\xi\eta$ plane

ANALYSIS OF SECOND MOMENTS

The second moments contain a wealth of information. The breakup time may be inferred from the run of either the dimensions or the orientation of fragment ensemble. The velocity dispersions may be obtained by assuming, as here, an ellipsoidal distribution. These dispersions give some indication, based solely on dynamical considerations, of the mechanism responsible for the breakup. To see why this is plausible, one can consider the two extreme possibilities of intentional, on-board destruction and destruction from the impact of a projectile. The former could likely yield a nearly isotropic velocity distribution, and the latter should yield a highly directional velocity distribution indicative of the angle of approach of the projectile.

The velocity dispersions will be considered first. Figure 12 shows the reciprocal square roots λ_i of the eigenvalues of matrix A. This matrix was calculated from equations (12) and (13), the second moments of the matrix J having been calculated from the relative positions according to the NAVSPASUR elements. These eigenvalues are constants in the theory. The variability evidenced in Fig. 12 may be attributed to observational error and the departure of the actual spatial density from the assumed ellipsoidal form. The largest of the λ_i varies the least and may be estimated to be 4.25 with an uncertainty of ± 0.1

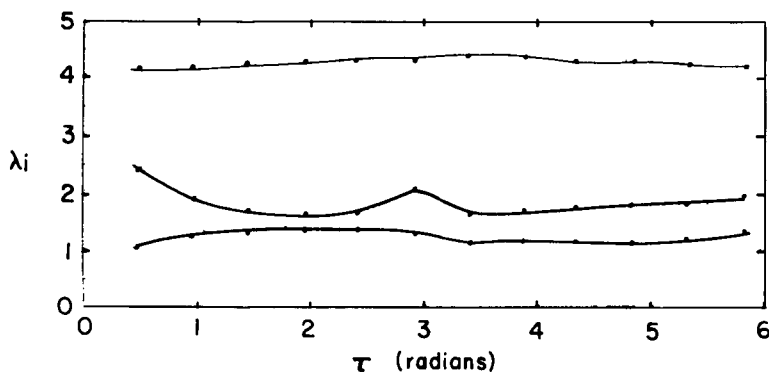


Fig. 12 — Reciprocal square roots of the eigenvalue of the calculated velocity dispersion matrix versus the true anomaly difference

(relative uncertainty 2.3%). The other two may be estimated to be 1.7 ± 0.3 and 1.20 ± 0.2 (relative uncertainty approximately 17% in both). This establishes the shape of the velocity ellipsoid to be roughly a prolate spheroid with aspect ratio 2.8:1. The orientation of the spheroid is determined by the eigenvector associated with the largest λ_i . Figure 13 shows the orientation angles of that eigenvector in the $e_1 e_2 e_3$ frame. There is considerable scatter about the mean values $\bar{\theta} = 31.1^\circ$ and $\bar{\phi} = 76.5^\circ$. The scatter places the direction of this eigenvector inside a cone whose axis is in the mean direction and with an apex angle of about 10° . The scatter in the other two eigenvectors is too large to permit a meaningful estimate of their directions. This may be attributed to observational error and to the computational ambiguity of finding the principal axes of an ellipsoid which is nearly a spheroid. The dot product of the unit vector associated with the mean direction of the principal axis (indicated by a cross in Fig. 13), namely $\bar{e} = (0.1927, 0.8233, 0.5168)$, and the unit vector associated with the mean velocity increment, namely $e = (0.1701, 0.7059, 0.6876)$, shows the angle between the two to be 12.4° . Thus the velocity ellipsoid is oriented roughly in the direction of the mean velocity increment. This shows that the Cosmos 699 breakup was highly directional. The mean velocity increment and the velocity ellipsoid are illustrated in Fig. 14.

The time of breakup follows from the second moments from both equation (16) and the discussion of it. A comparison of observed and calculated values for equation (16) are shown in Fig. 15. The amplitude is unimportant as far as the breakup time is concerned. This figure shows that the breakup time derived from the first moments is consistent with that obtained from the run of the dimension of the ensemble. No simple shift of origin would yield a better fit than shown.

CONCLUSIONS

First, some conclusions can be made with regard to the five outlying particles in Fig. 1a. The particle labeled 5 is merely a high-velocity particle ($\Delta v \approx 170$ m/s) which does

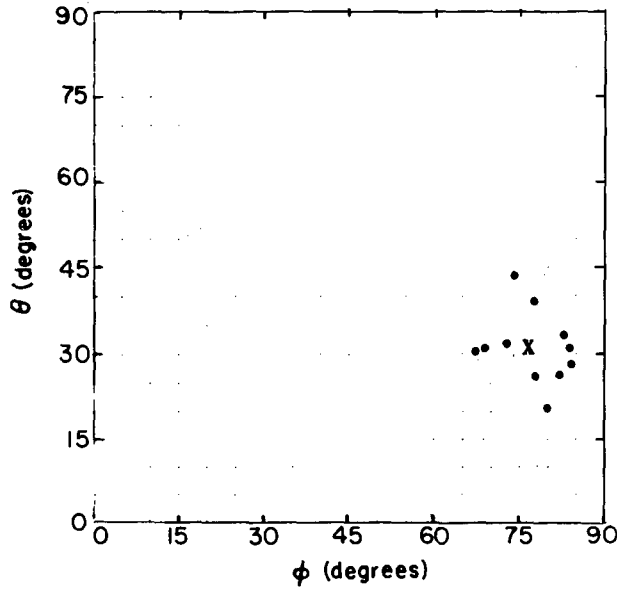


Fig. 13 — Orientation angles of the eigenvector associated with the largest λ_i

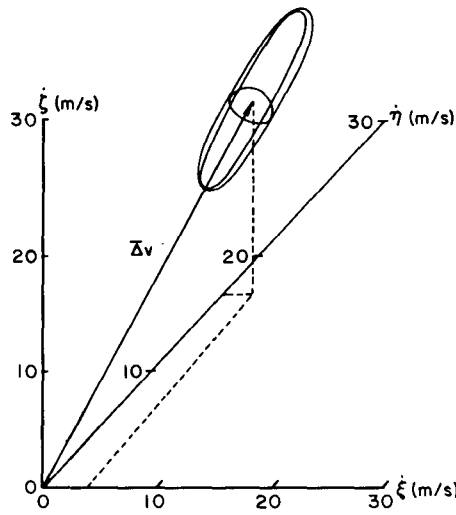


Fig. 14 — Illustration of the mean velocity increment and the velocity ellipsoid

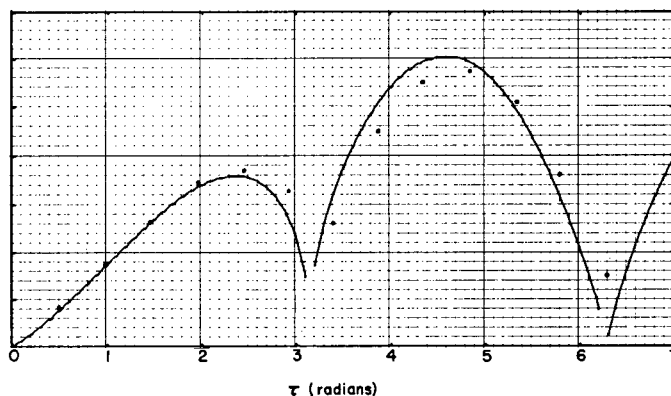


Fig. 15 — Function which determines the time of breakup from the matrix of second moments

originate with the main ensemble but evolves much more quickly. The remaining four particles however appear to have fragmented at different times. The relative trajectories of these particles (projected onto the $\xi\eta$ plane) are shown Fig. 16. The positions of the particles at breakup time are shown by large filled circles. When particle 1 is followed backward in time, it passes near the parent exactly two revolutions before breakup. If particles 2, 3, and 4 are followed forward, it is found that 2 and 4 pass near the parent exactly one revolution after breakup and particle 3 does so exactly 3 revolutions after breakup. It appears that these particles fragmented one and three revolutions respectively after the main breakup and did not even exist at breakup time. Their positions shown in Fig. 1a are purely fictitious. Another interesting observation is that all four epicycles leave roughly the same dimensions (as do their excursions out of reference plane) and that these in turn are typical of particles in the main ensemble. There is little doubt that they share a common fragmentation mechanism with the main ensemble. The scenario of a breakup is summarized on a ground trace in Fig. 17.

Second, some comments can be made with regard to the effectiveness of the theory. In spite of the facts that the eccentricity of the reference orbit is not zero (albeit small), that drag was included in the orbit calculations but not the statistical theory, and that a rather small sample size was available, the theory works remarkably well. An examination of Figs. 1a through 8a quickly convinces one that the actual spatial density is not ellipsoidal either, because of the apparent asymmetry along the major axis. Thus higher order moments would be necessary to describe the original velocity distribution in more detail. However, the computational difficulties encountered with the second moments indicates that one must anticipate trouble if such an attempt is made.

ACKNOWLEDGMENTS

I am particularly grateful to the NAVSPASUR system, especially Mr. R. Cote and Mr. R. Cox, for supplying the orbital elements used for the analysis and for several discussions about this breakup.

Fig. 16 — Positions of the exceptional fragments (Fig. 1a) relative to the payload as a function of time (projection onto the $\xi\eta$ plane)

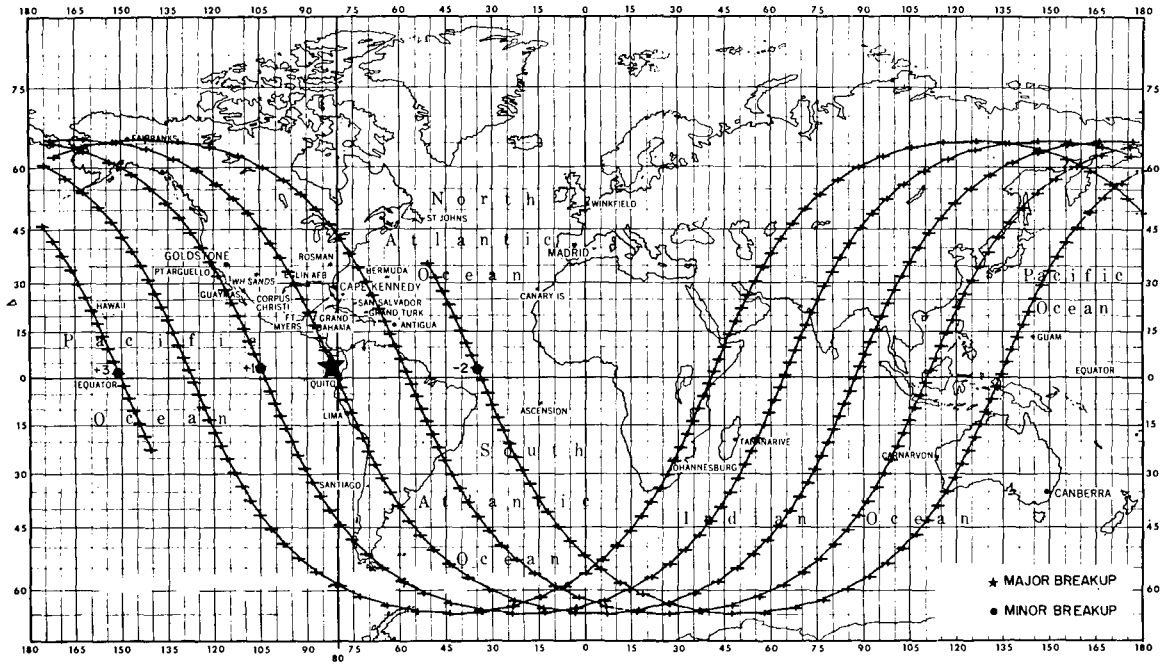
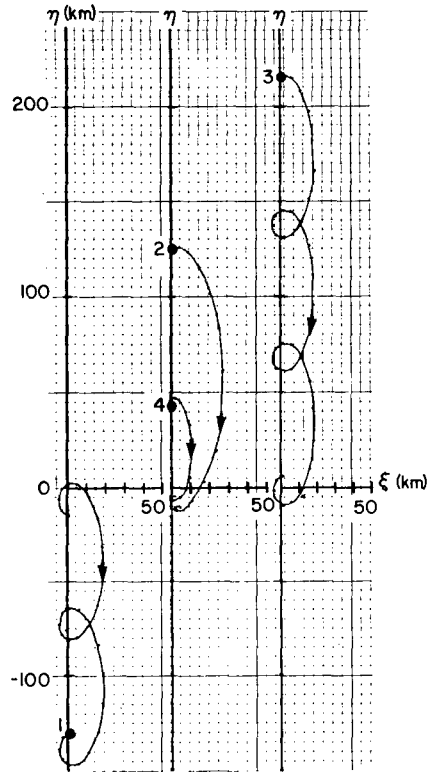


Fig. 17 — Ground trace for Cosmos 699

REFERENCES

1. W.B. Heard, "Dispersion of Ensembles of Non-Interacting Particles," accepted for publication in *Astrophys. and Space Sci.*, 1976.
2. B. Friedman, *Principles and Techniques of Applied Mathematics*, New York, Wiley, 1956.

